PHYSICAL REVIEW E VOLUME 59, NUMBER 3 MARCH 1999

Statistics and scaling behavior of chaotic domains in a liquid crystal light valve with rotated feedback

Eric Yao,[1,*] Francesco Papoff,[2] and Gian-Luca Oppo[1]
[1]*Department of Physics and Applied Physics, University of Strathclyde, Glasgow G4 0NG, United Kingdom*
[2]*Department of Physics and Astronomy, University of Manchester, Manchester M13 9PL, United Kingdom*

(Received 27 July 1998; revised manuscript received 23 November 1998)

An optical system containing a liquid crystal light valve and a two-dimensional feedback is known to form a wide variety of ordered and disordered spatial structures [Akhmanov *et al.*, J. Opt. Soc. Am. B **9**, 78 (1992)]. Here we describe a spatiotemporal feature—chaotic domains, obtained under temporal modulation of the input beam. We characterize these structures using a geometrical and a statistical approach. We find that the system retains low-dimensional dynamics locally while exhibiting spatiotemporal chaos. A power scaling relation between the size of the chaotic domains and the spatial coupling length of the system is also obtained from the experimental measurements. Good overall agreement is found between experimental results and the numerical integration of model equations. [S1063-651X(99)12803-4]

PACS number(s): 42.65.Sf, 42.79.Kr, 47.54.+r, 05.45.−a

I. INTRODUCTION

Since the pioneering experimental and theoretical works by Akhmanov *et al.* in the late 1980s [1–4] which are reviewed in Ref. [5], the liquid crystal light valve (LCLV) optical system with two-dimensional feedback loop has established itself as a prototype experiment in the field of pattern formation and instabilities in nonlinear optics [6–8]. It is a simple optical system with a high degree of flexibility and controllability, and is capable of generating a wide range of spatial and spatiotemporal distributions of light intensity.

In this paper we investigate the spatiotemporal dynamics of an optical system containing a LCLV with 180° rotated feedback and modulated input. Minimizing the effect of diffraction in the experiment by imaging the ''read'' side of the LCLV onto its ''write'' side, we consider diffusion and the rotation of the feedback as the main mechanisms for the spatial coupling. The rotation of the feedback by 180° and the modulation of the input field induce chaotic dynamics. Because of diffusion and the transverse boundaries (and experimental inhomogeneities), chaotic domains of in-phase dynamics are formed in different locations of the transverse space.

Without the modulation, the system is stationary for the given parameter settings. As the input beam intensity is increased, other complex spatiotemporal dynamics can be found even without the temporal modulation of the input. However, to the best of our knowledge the formation of bright chaotic domains is a particular feature not previously described within the rich phenomenology of this system.

We characterize the behavior of the system with a variety of techniques. Using Lyapunov exponents we show that the local dynamics in the domain is chaotic, and that the dynamics of the intensity of the entire pattern has a positive Lyapunov exponent which is lower than the exponents of the domains. Using statistical and geometrical techniques we also determine scaling laws in the time-averaged average size of the bright domains.

The paper is organized as follows: The experimental setup is presented in Sec. II. The model equation obtained by describing the propagation through all the optical elements of the experiment is discussed in Sec. III, together with the conditions to obtain temporal chaos. We also present numerical simulations of the full spatiotemporal chaos regime leading to the formation of the chaotic domains. Section IV presents the analysis of the experimentally observed spatiotemporal chaos, and presents evidence of a power scaling relation between the size of the chaotic domains and the spatial coupling length of the system. Conclusions and acknowledgements are contained in Sec. V.

II. EXPERIMENTAL SETUP

The setup for the experiment is shown in Fig. 1. The feedback fiber bundle is rotated by 180°, so that the feedback loop closes upon itself after two round trips of the system. The input light intensity is modulated by a Michaelson interferometer arrangement (boxed in the diagram of Fig. 1) with the mirror (M_{moving}) mounted on a piezoelectric crystal. An ac sinusoidal voltage is applied across the piezoelectric crystal to control the movement of the mirror. Since the movement is only a fraction of a wavelength, there is no loss of temporal coherence. This also ensures that the intensity of the output changes linearly with the displacement of the moving mirror. The input light intensity is continuously monitored, and a sample of the output signal of the monitoring photodetector is shown in Fig. 1. To influence the strength of transverse spatial coupling in the system, pinholes of varying sizes are used at position $P2$ to spatially filter the feedback beam. Photodiode detectors are used to monitor the temporal evolution of both the dynamics of a local spot in the transverse plane and the intensity of the entire output beam. The overall spatiotemporal behavior of the system is instead observed by means of a conventional video recorder. The images are then digitized and analyzed using a computer.

---

[*] Electronic address: eric@reynolds.ph.man.ac.uk

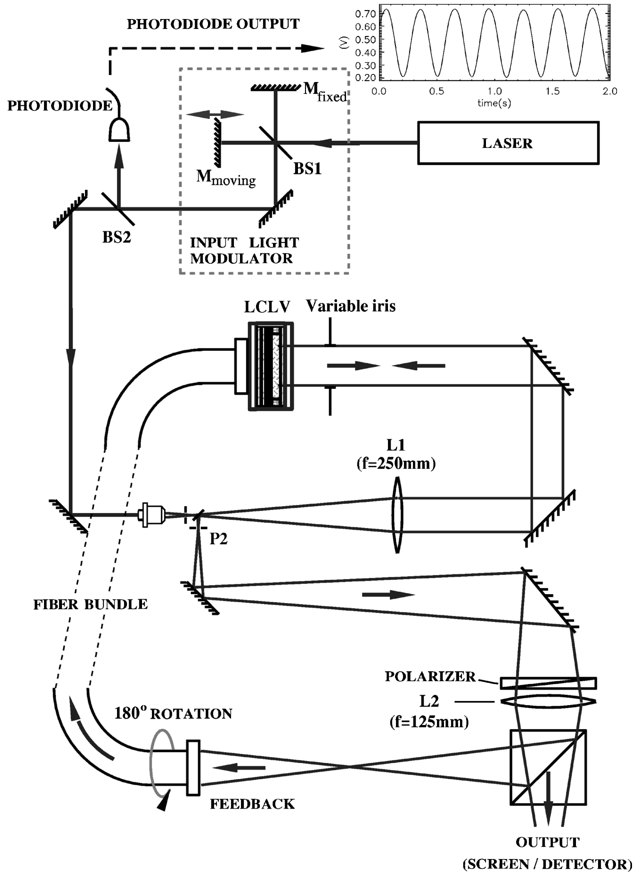

FIG. 1. Setup of the LCLV experiment.

III. SPATIOTEMPORAL CHAOS AND CHAOTIC DOMAINS IN THE MODEL EQUATION

Equations treating the LCLV as a nonlinear element inside an optical cavity have been derived in the past [9]. They successfully model and predict the behavior of an optical system similar to ours. There are, however, important factors that need to be taken into consideration. In our experiment the field transmitted by the fiber bundle is completely absorbed by the photoconductor layer. Moreover, the liquid crystal refractive index, which modulates the input light beam, is affected by the charge carrier density of the photoconductor and not by the field directly. Therefore, we have rederived the model equation by considering our experimental setup as a system with optical feedback. Although the final form of our model equation is similar to earlier models, our approach enables us to write the feedback coefficient and the strength of the nonlinearity in terms of experimentally measurable angles between the liquid crystal director, the polarizer orientation, and the direction of polarization of the input beam.

The model equation for our optical two-dimensional feedback system containing a LCLV is as follows:

$$\tau\frac{\partial\phi(\vec{r},t)}{\partial t}+\phi(\vec{r},t)=D^2\nabla^2\phi(\vec{r},t)+\kappa[1-\varepsilon\cos(ft)]\times[1+\gamma\cos(\phi(\vec{r}\,',t)+\phi_0)], \qquad (1)$$

where

$$\kappa=\mu BI_{\text{in}}/2[\cos^2(\psi_1+\psi_2)+\cos^2(\psi_1-\psi_2)],$$

$$\gamma=[\cos^2(\psi_1-\psi_2)-\cos^2(\psi_1+\psi_2)]/[\cos^2(\psi_1+\psi_2)+\cos^2(\psi_1-\psi_2)].$$

κ and γ are the strength of nonlinearity and the feedback coefficient respectively. ϕ is the phase shift of the read beam introduced by the LCLV, τ is the relaxation time constant, D is the effective diffusion coefficient, $\vec{r}\,'$ is $\vec{r}$ after coordinate transform through the feedback loop, and ϕ_0 is the constant phase shift. μ is the nonlinear coefficient of the LCLV, B is the total loss of the system, and I_{in} is the input light intensity. ψ_1 and ψ_2 are the angles between the liquid crystal director and the polarizer orientation and between the liquid crystal director and the direction of polarization of the input beam, respectively.

Notice that a modulation term has been included in this equation. f and ε are the frequency and depth of the modulation applied to the input beam, respectively. I_{in} appears in the expression for κ. Thus if I_{in} is of finite size κ will take on the same spatial profile as the pump beam. In our numerical simulations we use a pump beam with a top-hat shape with homogeneous intensity on the flat top. To model the feedback filtering pinhole numerically, the Fourier transform of the field is multiplied by a top-hat function. This is equivalent to a convolution in real space [10]. In the experiment diffraction is minimized by imaging the read side of the LCLV onto its write side; hence its effect is neglected in the model.

Without diffusion, Eq. (1) can be reduced to a set of two coupled nonlinear differential equations [1]:

$$\tau\frac{d\phi_1}{dt}+\phi_1=[1-\varepsilon\cos(ft)]\kappa[1+\gamma\cos(\phi_2+\phi_0)],$$
$$\tau\frac{d\phi_2}{dt}+\phi_2=[1-\varepsilon\cos(ft)]\kappa[1+\gamma\cos(\phi_1+\phi_0)], \qquad (2)$$

where ϕ_1 and ϕ_2 are the phase shifts at pairs of points x and x', connected through the 180° rotation of the feedback loop [11]. Equations (2) govern the temporal behavior of each half of the transverse field. The temporal behavior of this system, in the absence of modulation of the input light $(\varepsilon=0)$, is depicted by the phase diagram shown in Fig. 2. The symmetry of the diagram corresponds to the symmetry of the set of equations.

The location, number, and stability of the fixed points in Fig. 2 depend on the system parameters. One generic feature, however, is that the relaxations to the stable off-diagonal fixed points $(\overline{\phi_1},\overline{\phi_2})$ present damped oscillations, in agreement with the scaled eigenvalues of the linear stability

$$\Lambda=\tau[-1\pm\kappa\gamma\sqrt{\sin(\overline{\phi_1}+\phi_0)\sin(\overline{\phi_2}+\phi_0)}]. \qquad (3)$$

In particular, for the parameter values of Fig. 2, the relaxation oscillations have scaled frequencies of $3.44/(2\pi\tau)$, $5.42/(2\pi\tau)$, and $5.05/(2\pi\tau)$ for the stable fixed points *E, F*, and *G*, respectively. As the modulation of the input beam is introduced $(\varepsilon>0)$ at a frequency close to that of the damped oscillation, and its depth increased, a

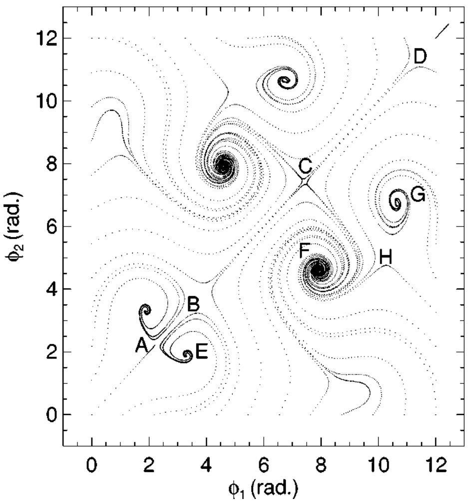

FIG. 2. Phase space diagram of the system: $\kappa=7.0$, $\gamma=0.82$, $\phi_0=0.338$, and $\varepsilon=0.0$. Points *A*, *B*, *C*, and *D* are saddle points along the diagonal. Away from the diagonal, there are symmetric pairs of stable fixed points corresponding to positions *E*, *F*, and *G*, while point *H* and its symmetric counterpart are saddle points.

complex chaotic attractor is formed in the region of phase space around the stable fixed points *E*, *F*, and *G*. Therefore, with suitable modulation of the input light intensity, chaotic dynamics can be induced in the bulk of the system.

Having found chaotic dynamics in the coupled o.d.e.'s [Eq. (2)], we extend our investigation to take spatial effects into account. By numerically integrating the original p.d.e. model equation [Eq. (1)] and monitoring pairs of transverse locations connected by the 180° rotation of the feedback loop, we can compare the dynamical behavior of the p.d.e. and the coupled o.d.e. systems (Fig. 3). In both cases we find that the strange attractors occupy the same region of space and have similar shape. The two distinct parts of the attractor are clearly identifiable in each of the two cases. The power spectra also show similar distributions of power in the frequency domain. There are, however, some differences between the two cases which become more pronounced as *D* increases. One of these differences is that the trajectories going around the higher suborbit are less spread out when diffusion is included. Another difference, less obvious from the diagram, is that when diffusion is present the orbit spends more time in the lower of the two suborbits. When *D* is sufficiently large, the dynamics will no longer be chaotic due to strong coupling to the boundaries of the beam where there is no oscillation at all. We avoid this ''large'' diffusion limit in our experiment.

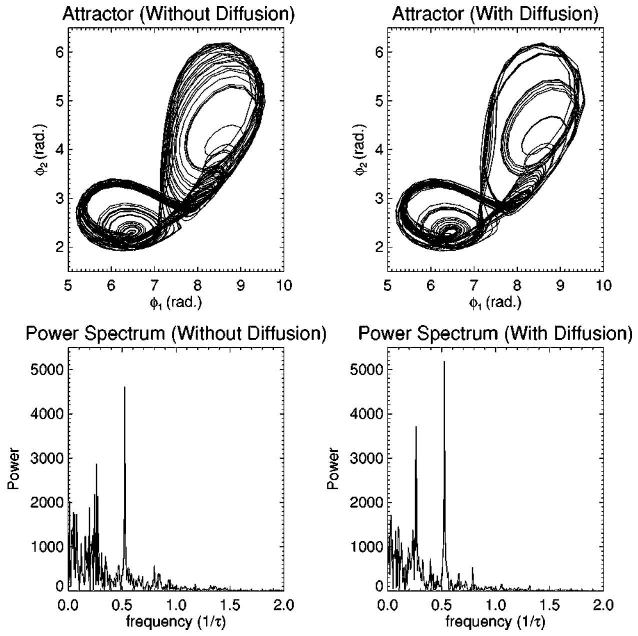

FIG. 3. Comparison of temporal dynamical behavior with and without diffusion. For the diffusive case, $D=0.03$. Frequency is normalized to the relaxation time of the LCLV.

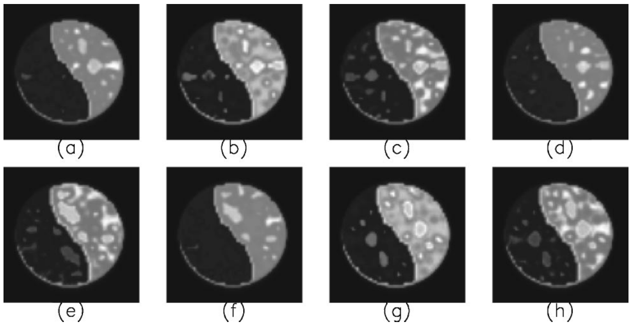

FIG. 4. Sequence of frames of the transverse profile of the diffusive system—numerical simulation. $\kappa=7.5$, $\gamma=0.82$, $\phi_0=2.338$, $\varepsilon=0.5$, and $f=0.526/\tau$, and the frame interval is 0.05τ.

The largest positive Lyapunov exponents, calculated from time series of each of the two cases, are

$$\lambda_{\max}=0.21\pm0.02 \quad (\text{without diffusion}),$$

$$\lambda_{\max}=0.22\pm0.02 \quad (\text{with diffusion}).$$

These values are in good agreement with each other, and also with the value of the largest Lyapunov exponent of the system, calculated from the o.d.e's, of 0.22 ± 0.01. For the purpose of these calculations the relaxation time of the LCLV is taken as unity.

Therefore, in the presence of diffusion, chaos induced in the bulk of the system is preserved. We note that the numerical results for the temporal characteristics of the diffusive case are independent of the transverse position so long as it is away from the boundaries of the pattern segment.

In the transverse plane of the system the beam is separated into two halves of unequal brightness, and within each of these halves there are bright spots. Figure 4 shows a sequence of snapshots [12] of the transverse beam profile showing the evolution of the complex spatiotemporal structures. Bright areas are shown to emerge from the darker surrounding background area, evolve in shape and size, and, then, collapsing onto themselves, disappear. New bright areas will then emerge elsewhere, and the sequence continues. We call the bright areas bright domains and the darker areas dark domains. These two types of domains occupy a common area away from the boundaries. We call this area the ''active region.'' Because bright domains are distinctive while dark domains are difficult to separate from the inactive areas, unless otherwise stated ''chaotic domains'' shall be used to refer to the bright domains. Rotational symmetry of

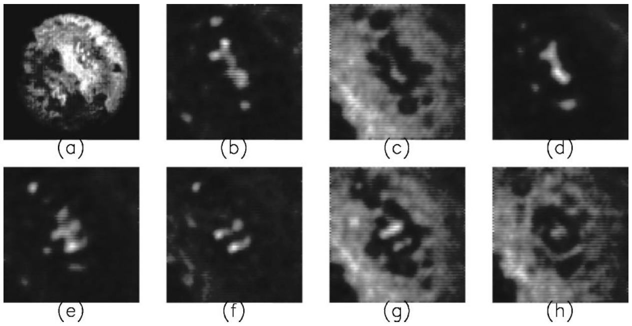

FIG. 5. Sequence of frames of the transverse intensity profile of the LCLV optical system—experiment (25 frames per second). Panel (a) shows the whole cross section of the beam while subsequent panels are enlarged portions showing the ''active'' region. The modulation frequency used here is 5 Hz.

the system is always preserved as these domains always evolve in pairs, one on either half of the beam. This is the case with all other spatial features. The average size and number of the bright domains is affected by the amount of diffusion in the system. The greater the diffusion the larger the size, and the smaller the number, of the domains. Therefore, the whole system behaves as a spatially extended array of interconnected subsystems evolving around the chaotic attractor where the subsystem size is affected by the amount of diffusion.

IV. EXPERIMENTAL OBSERVATION OF CHAOTIC DOMAINS AND STATISTICAL ANALYSIS

Based on the experimental observations, the diffusive model discussed in Sec. III appears to correctly predict the spatiotemporal behavior of our feedback system. When the experimental control parameters are set at the appropriate values suggested by the numerical simulation results, bright domains are observed [13]. Note that the response time of the LCLV ranges from some tens to hundreds of milliseconds depending on the controlling electronic signal. Therefore chaos is induced by using frequencies from 2 to 50 Hz for the modulation of the input light beam, in agreement with the relaxation oscillations observed with no modulation. Chaotic-type spatiotemporal dynamics and the formation of chaotic domains can also be observed, in the experiment as well as numerics, with higher (from 2–4 times) modulation frequencies although these dynamical regimes will not be dealt with in this paper. Figure 5 shows a sequence of snapshots of the enlarged ''active region'' of the beam. Each of these domains emerges from the darker surrounding background, oscillates, and changes its size, then contracts and dissolves away by collapsing into the center. This behavior is similar to the results of the numerical study. In the temporal domain, a chaotic-type behavior is observed, similar to that of the numerical simulations. The power spectrum of the time series is presented in Fig. 6. A broadband characteristic with substantial power in the low frequency components can be observed.

There are, however, some noticeable differences between the experimental observation and the numerical results. In the experiment, the bands of inactive region occupy a much broader area, so much so that the active region is confined to a relatively small area at the center of each half of the beam [see panel (a) of Fig. 5]. The shapes of the domains also appear to be more regular in the experiment as compared to the numerical results. As a consequence, although the sizes of the domains evolve in time, their shape does not appear to change significantly during their ''lifetime.'' There also seem to be preferential sites where chaotic domains are formed in the experiment, whereas in the numerical simulation domains are formed at random locations. This is probably due to spatial inhomogeneities in the experiment which are not included in the model equations.

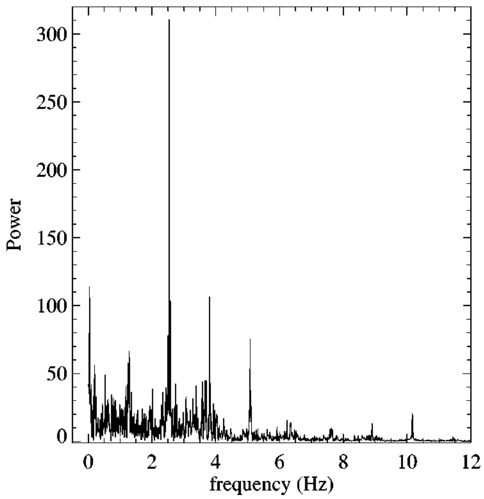

FIG. 6. Power spectrum of the experimental time series.

In the temporal domain, the method of delay coordinate embedding [14] was applied to the experimentally obtained time series of intensity measurement from a small area detector placed within the active region of the beam. We choose an embedding dimension of three since, from the numerical studies, we expect a three-dimensional space to be sufficient to unfold the attractor of interest to us. We also use the technique of singular value decomposition reduction [15] to reduce the effects of noise, as we expect the dynamics of the system to be low dimensional. Plotting the time-delay coordinates on this reconstructed phase space, we obtain the unfolded attractor shown in Fig. 7. Using the same technique, the numerically obtained time series of the diffusive case is also embedded. In the numerical case the time series is taken from monitoring ϕ within the active region. The dc part of each time series is removed since we are only interested in the dynamics.

Since the two orbits are reconstructed from time series of

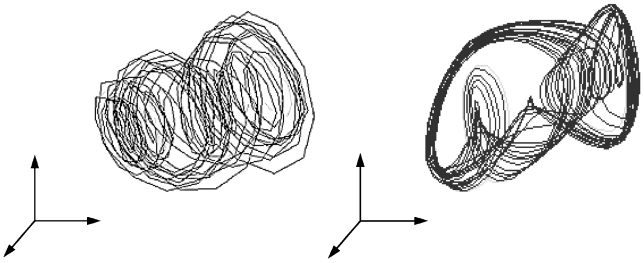

FIG. 7. Phase space portraits reconstructed using a delay embedding of time series data from the experiment (left hand panel) and numerical simulation of Eq. (1) (right hand panel).

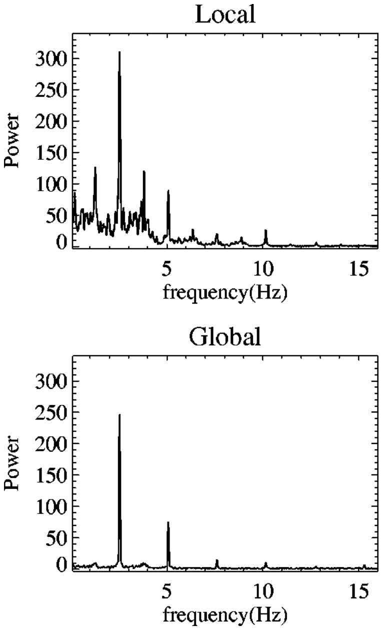

FIG. 8. Comparison of local and global power spectra (experimental result). The size of the pinhole used in filtering is 0.3 mm.

quantities which are closely related but not the same, they are not expected to be identical. However, in both cases the attractor unfolds in a three-dimensional space and resembles a coiled up spring, roughly separated into two interconnected parts. Although the experimental trajectories are not smooth, reflecting the limited sampling rate, and the flow of the trajectories is less well defined, reflecting the effect of residual noise, the two attractors are topologically similar objects. It is thus reasonable to conclude that the two reconstructed attractors originate from similar, if not the same, underlying dynamical systems. This is further supported by the measurements of the largest Lyapunov exponent which agree with one another.

A. Temporal characterization of the chaotic domains

In order to gain further knowledge of the relationship between the subsystems within the transverse cross section, we compare the dynamical behavior of the global system with that of the local system, and examine the differences between different types of local areas. By *local* we refer to a location within the active region of the transverse cross section of the system with an area much smaller than the typical size of the geometrical structures present. *Global*, on the other hand, means the total area of the transverse cross section. We characterize the differences in local and global behaviors by means of the power spectrum and the principal (largest) Lyapunov exponent.

The experimental results for these are given in Figs. 8 and 9. Figure 8 compares the power spectra of the experimental time series representing the two cases. A feedback filtering pinhole of 300-μm diameter is used. The power spectrum for the local behavior is broadband, with substantial power in the lower frequency region, clearly indicating that the behavior is chaotic. The power spectrum for the global behavior, however, indicates a mainly periodic oscillation with a number of isolated peaks. Only a small amount of power is distributed among other frequencies. Although the global behavior is clearly dominated by the modulation of the input beam (the dominant frequency in the power spectrum corresponding to the driving frequency of the input beam), the largest Lyapunov exponents are small but still positive, indicating chaotic oscillation.

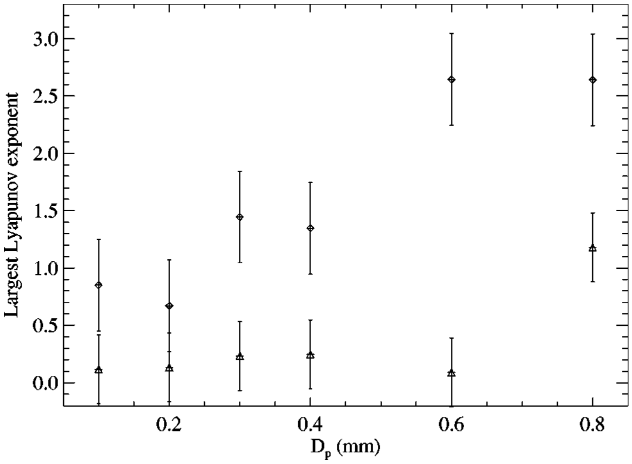

FIG. 9. Largest Lyapunov exponents of local (diamonds) and global (triangles) intensity (experimental result).

For the calculation of the largest Lyapunov exponent, the measurements are repeated with different sizes of pinhole for the varying strength of the spatial coupling of the system. It is found that the dynamics at the local level is consistently more chaotic than its global counterpart throughout the range of pinhole size (Fig. 9).

The largest Lyapunov exponents of the local variable are found to increase as the diameter of the feedback pinhole is increased, suggesting that with weakening spatial coupling the subsystems become less synchronized with one another. As a result they can oscillate more independently of each other, becoming more chaotic in the process. This relation between the chaoticity and the spatial coupling is also found for the global dynamics.

These observations are supported by the numerical results. The variation of the principal Lyapunov exponent with pinhole size (inversely proportional to spatial coupling strength) is shown in Fig. 10. In the pinhole diameter range

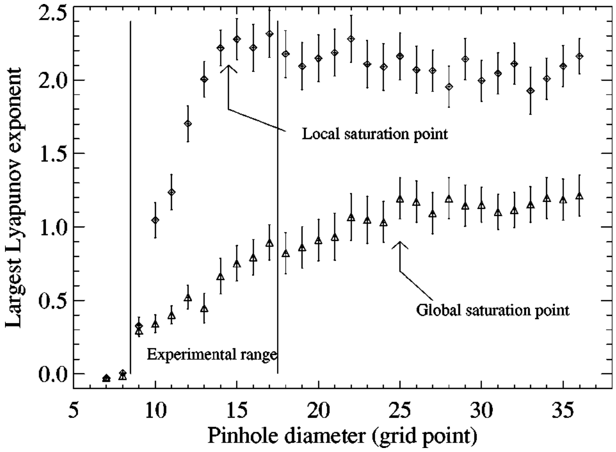

FIG. 10. Largest Lyapunov exponents of the local (diamonds) and global (triangles) systems (numerical simulation).

corresponding to the experimental values, shown in Fig. 10, the same behavior is observed both numerically and experimentally.

In the numerical simulation a much wider range of pinhole size can be explored than is possible in the experiment. We find that as the pinhole size is increased there is a ''saturation'' of the largest Lyapunov exponent for the local system [starting at a pinhole diameter of 15 (in units of grid separation), $D_p = 15$]. This is in agreement with other studies of extended chaotic systems [16], where it is found that for a *large* extended system the largest Lyapunov exponent of the subsystem is an *intensive* quantity, i.e., not dependent on the size of the system. For pinholes smaller than this saturation point the criterion of a *large* system is not fulfilled—the subsystems are still strongly coupled to each other.

Saturation is also found in the global system, but at larger pinhole size $(D_p > 25)$. In this case saturation occurs because, beyond a certain size of pinhole, only the highest spatial frequencies are affected. Filtering at this point is no longer effective as a way of changing the spatial coupling strength of the system—diffusion has taken over as the dominant mechanism of spatial coupling.

B. Statistics of the domain size

Having discussed the variation of dynamics at different spatial locations, we now look at the domains themselves in relation to the change of experimental parameters. In the results of the numerical simulations the average size of the chaotic domains varies with diffusion. Diffusion cannot be varied significantly in the experiment, and consequently we are not able to verify this numerical result. However, since diffusion plays the role of spatial coupling, the strength of spatial coupling can be varied in the experiment by spatially filtering the feedback pattern. We can now measure the dependence of domain size with the pinhole size of the spatial filter.

At a given moment in time there may be a number of domains with varying sizes. We measure the time-averaged mean value of the domains sizes, $\langle s \rangle$, as well as the standard deviation and skewness of the distribution of the sizes. Using the digitized video images of the output beam, a threshold value for the intensity is set, and pixels brighter than this threshold value are considered to be part of a domain. In this way the number of domains and the area of each are measured. The experimental and numerical results are shown in Fig. 11.

In the experiment, the average size of the domains is found to reduce with the increase of pinhole size while the total domain area remains constant [Fig. 11(a1)]. Hence reducing spatial coupling breaks up the domains. There is, however, an exception to the rule which occurs at the point of the largest pinhole size [Fig. 11(a1)]. We label that as a ''turning point.'' The graph is plotted on a log scale to show the exponential relation between the diameter of the pinhole and the domain size.

The variation of the standard deviation of domain size with pinhole size follows the general trend of the average domain size [see Fig. 12(a2)]. When the average size of the domains is small, the difference between the sizes of individual domains is also found to be small. In the case of skewness [see Fig. 11(a3)] the value is always positive, which means that the distribution of values is more spread out above the mean. The skewness increases when the average size of the domain reduces, reflecting the fact that the mean is moving closer to the lower cutoff value of zero. There is also a turning point in the skewness of the distribution of the domain sizes. This shift in the shape of the distribution takes place before the turning behavior of the mean.

The results of the numerical simulations [Figs. 11(b1)–11(b3)] are in agreement with the experimental observations. Within the range of pinhole size corresponding to the experiment, $(10 < D_p < 17)$, the same behavior is observed. In particular, as the pinhole diameter increases, the average size of the domains and the standard deviation decreases while the skewness increases. We can also observe the turning behavior of the mean and the skewness, the latter preceding the former as D_p gradually increases. When D_p is increased beyond the two turning points, the skewness begins to fluctuate. This coincides with small values of standard deviation, and is a reflection of the fact that when the spread of a measured value around its mean is small the shape of the distribution can be easily affected by fluctuations of the individual measurements.

From the numerical results we can identify different types of relations which exist between the pinhole diameter and the size of the chaotic domains. We illustrate this by plotting the results of a typical numerical study; see Fig. 12. Since this is a representative picture, in the future we shall refer to the range of size of pinholes as corresponding to regions A, B, and C.

Region A corresponds to the condition where chaos cannot be sustained due to the strong spatial coupling. This region is of no special interest to us in terms of the study of spatiotemporal disorder. In region C the effect of spatial filtering is weak compared with other coupling mechanisms such as diffusion. Changing the size of the pinhole in this region will have no effect on the spatiotemporal dynamics of the system, and so the basic feature in this region is a flat line. In region B, the average size of the chaotic domains is found to depend strongly on the diameter of the filtering pinhole. Within this range, spatial filtering of the feedback pattern is clearly an effective way of changing the complexity of our system.

There is one other feature of this ''typical'' picture—the dip at the turning point. Since if too large a pinhole is used it will not be effective in spatial filtering, we expect that as the size of the pinhole increases the size of the domains should gradually decrease toward a constant value dictated by the diffusion coefficient. However, at the boundary of regions B and C there is a small range of pinhole size within which the average domain size is smaller than that within either of the two regions. If we consider the dominant spatial coupling mechanism in regions B and C to be spatial filtering and diffusion, respectively, then in this border area our results suggest that spatial coupling is in fact weaker when the two mechanisms are combined.

C. Scaling of chaotic domain size with spatial coupling

In Sec. IV B the average domain size was shown to change with the size of the pinhole. Within this filtering ef-

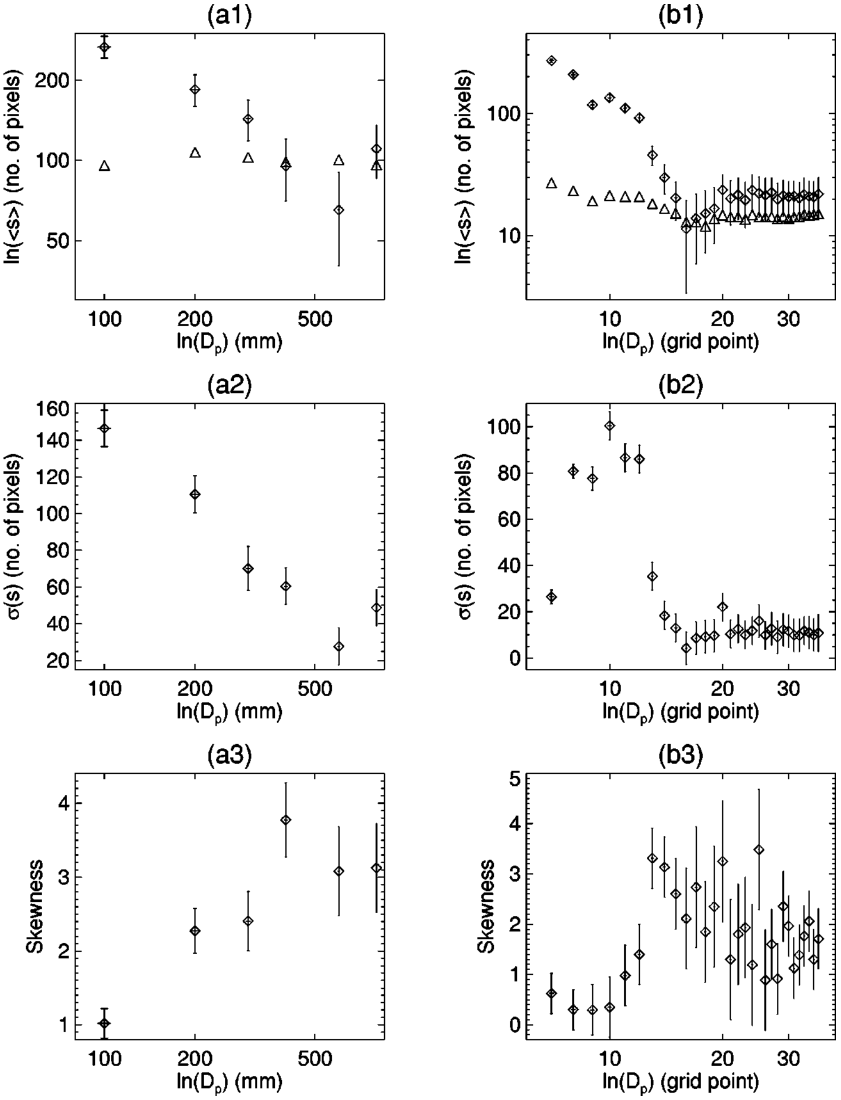

FIG. 11. Statistics (mean, standard deviation and skewness) of the time-averaged size of chaotic domains vs the log of the pinhole diameter, D_p. Plots on the left hand side [(a1)–(a3)] are experimental results. Numerical results are on the right hand side [(b1)–(b3)]. In the experimental graphs, D_p is in units of μm, while for the numerical curves D_p is in units of the grid separation, normalized to the diffusion length. Note the variation of the total area of the bright domains, 10% of Σs, is shown as triangles on the same plots as for $\langle s \rangle$ [panels (a1) and (b1)].

fective region (region B) a power scaling behavior between $\langle s \rangle$ and D_p emerges. In this subsection we examine region B, and try to understand the underlying mechanism for this scaling behavior.

Diffusion and spatial filtering are the two mechanisms in our system which affect the coupling between neighboring spatial points. They are associated with their corresponding length scales, namely, diffusion length L_{dif} and spatial filtering length L_{filter}. L_{dif} can be measured directly from the experiment, and is proportional to the diffusion coefficient D in the model equation (1). L_{filter} is inversely proportional to the diameter of the pinhole, D_p.

In our experiment diffusion cannot be varied effectively. Therefore, the effect of changing diffusion is studied numerically. We find that both diffusion and spatial filtering affect the average size of the chaotic domains. This can be seen in Fig. 13, where we plot the average domain size versus pinhole diameter for diffusion coefficients $D=0.1$ and 0.01. The position of the turning point of $\langle s \rangle$ and the length and posi-

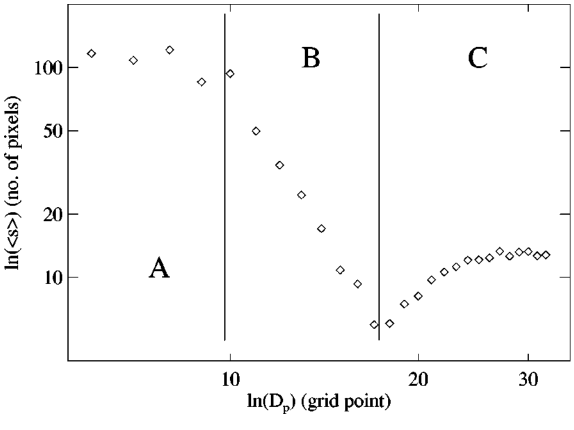

FIG. 12. Variation of the average domain size with pinhole diameter (numerical result). Three regions marked A, B, and C, showing different types of relationships, can be identified. (Diffusion was set at $D=0.8$.)

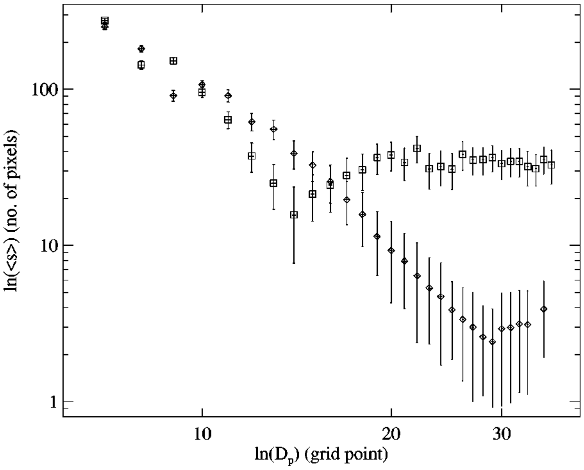

FIG. 13. Scaling of the average domain size with pinhole diameter (numerical). Two curves correspond to two different values of diffusion: $D=0.10$ for the squares and $D=0.01$ for the diamonds.

tion of the filtering effective region (region B) are both affected by diffusion. The value to which $\langle s\rangle$ converges when D_p is large also changes with diffusion, as shown in Fig. 14.

These observations lead to the conclusion that the average size of the domains is a function of the two length scales, i.e., $\langle s\rangle = f(L_{\mathrm{dif}}, L_{\mathrm{filter}})$. From dimensional considerations we expect this function to consist of terms of the form $L_{\mathrm{dif}}^{2-\beta} L_{\mathrm{filter}}^{\beta}$, because $\langle s\rangle$ has a dimension of length squared. Therefore, to the first approximation we can write

$$\langle s\rangle = \alpha L_{\mathrm{dif}}^{2-\beta} L_{\mathrm{filter}}^{\beta}, \tag{4}$$

where α contains information about the geometry of the domains, and β measures the relative importance of the length scales.

If this approximation is valid then the power scaling of $\langle s\rangle$ with L_{filter} and L_{dif} will be reflected as straight lines in the log scale plots of $\langle s\rangle$ versus the two length scales. The numerical results in Figs. 13 and 14 show that there are regions of the curves in which linear relations between $\ln(\langle s\rangle)$ and D_{filter} and between $\ln(\langle s\rangle)$ and L_{dif} exist. The experimental plot of $\ln(\langle s\rangle)$ versus D_p (Fig. 15) clearly shows that the data points fall mainly within region B. A straight line can be fitted through all the data points except for the points when pinhole size is 800 μm, exhibiting the turning behavior observed in the numerical results. The slope of the line is measured to be $\beta = 0.95 \pm 0.1$. From the experimental result we may conclude that the average size of the chaotic domains scales linearly with the diffusion length as well as with the length scale associated with spatial filtering. This seems to be supported by the numerical plot of $\ln(\langle s\rangle)$ versus D_{dif} when filtering is less effective (Fig. 14). Here the slope is also close to 1 $[(2-\beta) = 1.08 \pm 0.1]$. Combining numerical and experimental results, we can write

$$\langle s\rangle \simeq \alpha L_{\mathrm{dif}} L_{\mathrm{filter}}. \tag{5}$$

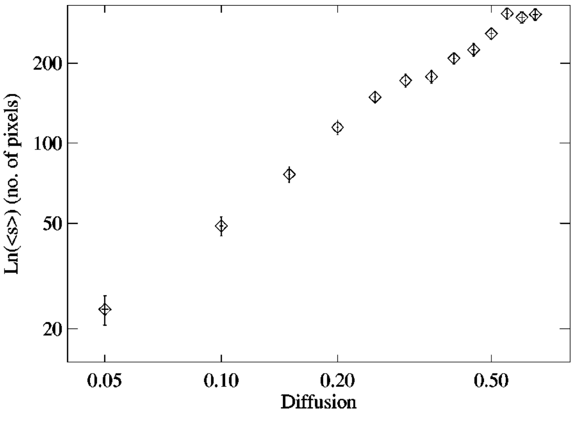

FIG. 14. Average domain size vs diffusion (numerical).

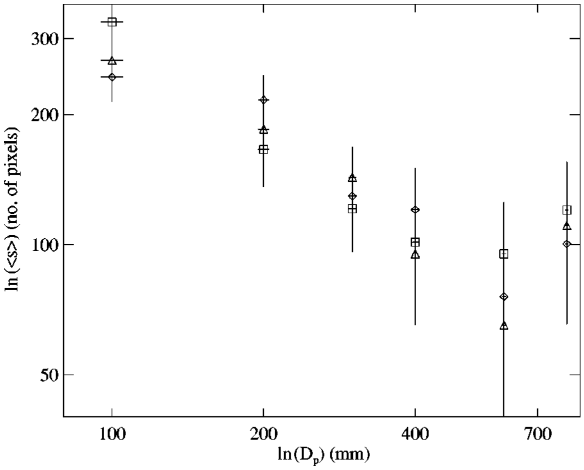

FIG. 15. Scaling of the average domain size with pinhole diameter (experimental).

This states that the chaotic domains are of a geometrical shape with two scaling lengths. The simplest example of this would be a rectangle or an ellipse. More complex geometrical structures may have more length scales, and the log scale power relation plot may not always have a slope (β) which is an integer.

The numerical picture is in fact more complicated than it at first appears. As the pinhole size changes, the slope of $\ln(\langle s\rangle)$ versus diffusion also changes. This variation is shown in Fig. 16. In region B, where filtering is effective, β fluctuates and does not have an integer value. This reflects the

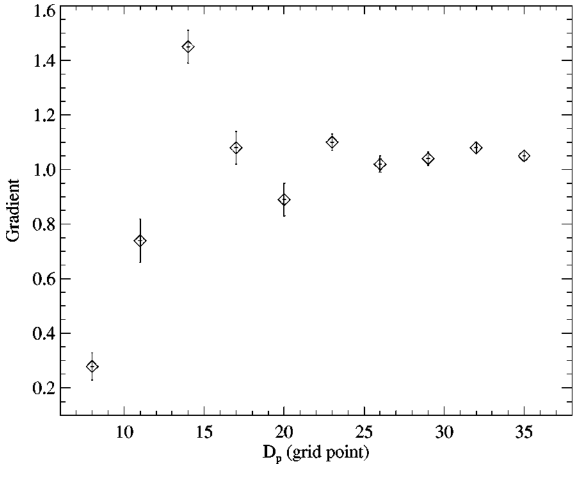

FIG. 16. Variation of the slope of $\ln\langle s\rangle$ vs diffusion (of which Fig. 14 is an example) with D_P (numerical).

complex nature of the chaotic domains in this region. As the pinhole size increases, in region C, the slope converges to a value close to 1.0.

These intriguing differences between the numerical and experimental results are subjects open to further investigation. Although introducing spatial filtering in the experiment has the desired effect of changing the strength of the spatial coupling, far more complex changes take place. The lack of homogeneity in the experiment, the diffraction introduced by the pinholes, and fluctuations in the modulation of the input beam (in time as well as in space) are all effects which are not accounted for in our model. Nonetheless, the model is effective in recovering the power relation between $\langle s \rangle$ and the filtering length.

V. CONCLUSION

In this paper we have investigated the spatiotemporal dynamics of a LCLV system with two-dimensional feedback and a modulated input beam. Spatiotemporally chaotic dynamics is found for a wide region of input modulation. This regime is characterized by the formation of bright chaotic domains. By evaluating Lyapunov exponents and power spectra, we found—both in experiments and in numerical simulations—that the local chaotic dynamics remains low dimensional while the global dynamics is dominated by the periodic modulation of the input light. The degree of complexity of the system is found to be a function of the transverse spatial coupling strength. From the statistical measurements of the average size of the chaotic domains, we uncovered a scaling relation between the average size of the chaotic domains and spatial coupling strength. In particular, these chaotic domains are found to be affected by two length scales: one relating to the spatial filtering of the feedback and the other to diffusion.

Characterization of spatiotemporal disorder in regimes of developed turbulence in optical systems is still an open field of research. We have shown, however, that standard statistical techniques can be successfully applied to regimes of weak optical turbulence when the mechanism underlying the spatiotemporal disorder is clearly defined. In our case the bulk chaotic oscillations induced by the temporal modulation of the input beam couple with the spatial coupling due to diffusion. When these two mechanisms have comparable strengths, well-defined out of phase chaotic domains occur introducing loss of spatiotemporal correlations. Possible generalizations include the effect of diffraction (here neglected but often impossible to eliminate completely in optical experiments) and the utilization of faster optical nonlinearities. We leave these research subjects to future communications.

ACKNOWLEDGMENTS

E.Y. and F.P acknowledge financial support from EPSRC (Grant No. GR/M 17983). F.P. acknowledges financial support from the European Union. G.-L.O. acknowledges financial support from EPSRC (Grant No. GR/M 19727).

---

[1] S. A. Akhmanov, M. A. Vorontsov, V. Y. Ivanov, A. V. Larichev, and N. I. Zheleznykh, J. Opt. Soc. Am. B **9**, 78 (1992).

[2] S. A. Akhmanov, M. A. Vorontsov, and V. Y. Ivanov, JETP Lett. **47**, 707 (1988).

[3] M. A. Vorontsov, N. I. Zheleznykh, and V. Y. Ivanov, Opt. Quantum Electron. **22**, 501 (1990).

[4] S. A. Akhmanov, A. V. Larichev, and M. A. Vorontsov, in *Coherence and Quantum Optics* (Plenum, New York, 1990), Vol. I, pp. 23–27.

[5] *Self-Organization in Optical Systems and Applications in Information Technology*, edited by M. A. Vorontsov and W. B. Miller (Springer, Berlin, 1995).

[6] M. A. Vorontsov, N. G. Iroshnikov, and R. L. Abernathy, Chaos Solitons Fractals **4**, 1701 (1994); F. T. Arecchi, A. V. Larichev, and M. A. Vorontsov, Opt. Commun. **105**, 197 (1994).

[7] F. T. Arecchi, A. V. Larichev, P. L. Pamazza, S. Residori, and J. C. Ricklin, Opt. Commun. **117**, 492 (1995); E. Pampaloni, P. L. Ramazza, S. Residori, and F. T. Arecchi, Phys. Rev. Lett. **74**, 258 (1995).

[8] B. Thuring, R. Neubecker, and T. Tschudi, Opt. Commun. **102**, 111 (1993); R. Neubecker, B. Thuring, and T. Tschudi, Chaos Solitons Fractals **4**, 1307 (1994).

[9] M. A. Vorontsov, Y. D. Dumarevskii, D. V. Pruidze, and V. I. Shmal'gauzen, Izv. Akad. Nauk SSSR, Ser. Fiz. **52**, 374 (1988).

[10] E. V. Degtiarev and M. A. Vorontsov, J. Mod. Opt. **43**, 93 (1996).

[11] E. Pampaloni, S. Residori, and F. T. Arecchi, Europhys. Lett. **24**, 647 (1993); P. L. Ramazza, E. Pampaloni, S. Residori, and F. T. Arecchi, Physica D **96**, 259 (1996).

[12] E. Yao, F. Papoff, and G.-L. Oppo, Opt. Commun. **115**, 73 (1998).

[13] E. Yao, Ph.D. thesis, University of Strathclyde, 1997.

[14] N. H. Packard, J. P. Crutchfield, J. D. Farmer, and R. S. Shaw, Phys. Rev. Lett. **45**, 712 (1980).

[15] D. S. Broomhead and G. P. King, Physica D **20**, 217 (1986).

[16] M. C. Cross and P. C. Hohenberg, Rev. Mod. Phys. **65**, 851 (1993); M. C. Strain and H. S. Greenside, Phys. Rev. Lett. **80**, 2306 (1998).